ACS OMEGA

http://pubs.acs.org/journal/acsodf

Article

Microstructural and Sensitivity Changes of Neat, Spray-Dried RDX

Jeremy T. Tisdale,* Brian L. Scott, Chris E. Freye, Larry G. Hill, and Amanda L. Duque*

Cite This: *ACS Omega* 2023, 8, 1514−1522

Read Online

ACCESS | Metrics & More | Article Recommendations | Supporting Information

ABSTRACT: Spray drying has recently gained interest in the high explosives (HE) community for the production of novel nanocomposites and well-controlled particle size distributions. However, there is a dearth of information on spray-dried, neat energetic materials. In this work, we correlate the spray drying production parameters to the resulting microstructure and handling sensitivity properties of neat RDX. We demonstrate the capability to fine-tune the particle size distributions for "nanopowder" spray-dried RDX, as well as larger particle size distributions by simply changing the spray dryer setup. We also investigate other physical and chemical changes that RDX undergoes after being processed with spray drying. We characterize these changes with scanning electron microscopy, X-ray diffraction, ultrahigh-performance liquid chromatography, and small-scale sensitivity tests. Interestingly, although the phase and chemical properties are similar before and after spray drying, small-scale sensitivity testing reveals that size reduction of RDX does not follow the typical HE desensitization trends, generally observed for other energetic materials.

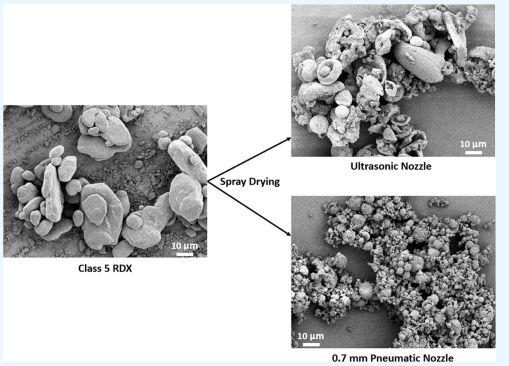

1. INTRODUCTION

Spray drying has been used for decades as a cost-effective production technique for micro/nanoparticles, as well as microencapsulation.[1−3] This processing technique has been widely studied in the food and pharmaceutical industries,[4−8] and has recently been applied to high explosives (HE). Methods to control particle size, void fraction, and void structure are important for reducing the sensitivity of HE composites,[9−16] and spray drying has shown promise for controlled production of ultrafine, narrow particle size distributions (PSD) that are difficult to achieve with traditional HE processing techniques, such as mechanical milling, grinding, and recrystallization.[17−20]

Previous work of others has demonstrated that spray drying of HE composites produces novel energetic material microstructures, including micro/nanocomposites,[21−27] cocrystals,[28,29] and novel energetic formulations.[30−33] While spray drying has proven to be a cost-effective, simple processing method for HE composites, few studies have focused on utilizing spray drying to process neat (single-component) HE materials.[34,35] Recently, we demonstrated the ability to produce pentaerythritol tetranitrate (PETN) nanocrystals with a narrow particle distribution, which is generally understood to be a strategy for controlling the sensitivity of energetic materials. Indeed, we showed that spray drying standard, crystalline PETN into an ultrafine PSD with smooth crystal facets significantly reduced the small-scale handling sensitivity.[35] However, some studies have shown that reduction of crystal size can also lead to increased sensitivity for certain energetic materials,[36,37] which makes understanding sensitivity properties in connection with material microstructure an important and complex issue.

In this work, we investigate the production of nanocrystalline 1,3,5-trinitro-1,3,5-triazinane (RDX) via spray drying. We focus on processing and characterizing neat, spray-dried RDX, whereas others have reported RDX-based nanocomposites with polymeric binders.[22,23,37,38] Here, we investigate the microstructure of RDX before and after spray drying and how important properties are influenced by these microstructural changes. We show that spray drying may be used to accurately control the PSDs of powders, and how variations in the setup will produce morphological as well as small-scale sensitivity changes. Along with other sensitivity studies on nanoscale RDX, we also show nanopowder RDX (average particle size of 0.57 μm) is more sensitive in small-scale sensitivity tests in response to impact and friction stimuli compared to Class 5 RDX (average particle size of ∼30 μm),[39] which is the smallest RDX powder that is commercially available.[36,37]

2. EXPERIMENTAL SECTION

2.1. Materials and Processing. The source RDX used in this work is Class 5 RDX, which is a commerical lot of material purchased from Holston Army Ammunition Plant. The source

Received: October 31, 2022
Accepted: December 14, 2022
Published: December 27, 2022

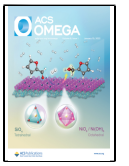

RDX was first dissolved in acetone, at 5% by weight. For the 0.7, 1.4, and 2.0 mm nozzle spray-dried RDX, a two-fluid nozzle system in a Buchi B-290 spray dryer was used to process the solution, with variations in the nozzle opening size as specified. A detailed description of the process and setup is given in our previous work.[35] Using the pneumatic two-fluid nozzles, the feedstock solution is co-sprayed through the system with heated nitrogen gas. As the solution sprays, the heated nitrogen gas evaporates the solvent from the atomized droplets. The resultant product is a fully dried powder RDX.

When using the ultrasonic nozzle during spray drying, the process of creating droplets is different. Rather than the pneumatic atomization for the two-fluid nozzles, the ultrasonic nozzle breaks apart the solution into droplets using ultrasonic vibrations. This process creates much larger droplets than the pneumatic nozzles, which in turn results in larger particles being processed after spray drying. A Buchi B-295 inert loop is used to process in an inert atmosphere. In both cases, no further post-processing techniques occur after spray drying, as this process controls the particle size distribution and fully dries the RDX powder to be used immediately after spray drying.

2.2. Materials Characterization. Scanning electron microscopy (SEM) images were acquired on a JEOL 7900F field emission microscope taken with the lower electron detector emission capture. The samples were prepared by first dispersing a microgram quantity of material onto a standard SEM aluminum stub by wetting with hexane. After the hexane had fully evaporated, a 4 nm layer of Au/Pd (80:20) was applied with a sputter coater to reduce charging and to enhance emission during imaging.

Particle size distribution (PSD) of spray-dried powders was achieved by high-resolution image analysis using a Keyence VK-1000 3D laser confocal microscope and its built-in particle size analysis software. Using this method, we imaged and compiled sample sizes of ∼2000 particles per sample for number-based statistical analysis.[40] During image analysis, agglomerates were removed from sampling to calculate PSDs based on singular particles. Due to the sample sizes used in the image analysis method, we utilized a continuum statistics method to derive a probability distribution function to best describe the PSDs for each spray-dried RDX sample. A detailed explanation of this statistical method is fully explained in our previous work.[35]

Surface area measurements were taken on a Quantachrome ASiQ3 (Quantachrome Corporation) in large glass bulb cells with a 6 mm stem. Liquid nitrogen (77 K) was used as the coolant. The specific surface area was calculated using the Brunauer−Emmett−Teller (BET) method, determined by the physical adsorption of nitrogen onto the surface of the sample at 77 K. Prior to measurement, the sample was degassed for 1 h to remove any impurities.

For XRD experiments, samples were pressed, without further processing, onto a silicon, zero background plate. The data were collected on a Bruker D8 Advance, with Ni-filtered Cu radiation (K_{ave}= 1.5418 Å) and a Lynxeye 2D silicon strip detector. Data analysis was performed using JADE Powder XRD Analysis Software [ref: JADE v. 8.2, 2021, Materials Data Incorporated, Livermore, CA]. Crystallite size and strain were determined from whole pattern refinements of the diffraction patterns.

For ultrahigh-performance liquid chromatography (UHPLC), acetonitrile (HPLC Plus) was obtained from Sigma-Aldrich. Ammonium acetate was obtained from VWR and was diluted to 10 mM using deionized water (HPLC PLUS) obtained from Sigma-Aldrich. RDX samples were dissolved in acetonitrile at a concentration of ∼50 μg/mL. The samples were put on a wrist shaker for 30 min to aid dissolution. A standard for HMX was prepared with an ultrapure HMX lot (less than 0.1% RDX) using acetonitrile at ∼400 μg/mL, which was further diluted using acetonitrile to concentrations ranging from ∼20 to ∼625 ng/mL. The samples were analyzed via a Shimadzu UHPLC system (Shimadzu, Japan) coupled with a SCIEX 3500 QQQ (SCIEX, Framingham, MA). The UHPLC system consisted of two binary pumps (LC30-AD), a degasser (DGU-30A), a column oven (CTO-20A), and an autosampler (SIL-30A). The QQQ system was equipped with an electrospray ionization (ESI) source that was operated in negative mode. The ESI conditions were as follows: ion spray voltage −4.5 kV, temperature 275 °C, ion source gas #1 20 psi, ion source gas #2 20 psi, declustering potential −10 V, and CAD gas 8 au. The multiple reaction monitoring (MRM) parameters are shown in Table 1.

Table 1. MRM Parameters for UHPLC Measurements

compound	Q1	Q3	DP	CE	CXP
HMX	355	46	−35	−34	−5
RDX	281	46	−20	−22	−11

Melt temperatures and thermal decomposition temperatures were measured by DSC (TA Instruments Q2000 DSC) in hermetically sealed aluminum pans that contain a pinhole lid. A typical analysis utilizes approximately 1 mg of sample with 50 mL/min ultrahigh-purity nitrogen purge gas at a thermal ramp rate of 10 °C/min.

2.3. Small-Scale Sensitivity. Small-scale sensitivity comparisons were investigated between the Class 5 RDX, 0.7 mm nozzle spray-dried RDX, and ultrasonic nozzle spray-dried RDX, as these three materials had vastly different morphologies and PSDs. Impact sensitivity was measured with a drop hammer LANL Explosives Research Laboratory (ERL) Type 12b test (no grit) on ∼40 mg of powder with a 0.8 kg striker, 2.5 kg weight, and sound detection equipment. The Neyer D-Optimal method was used to determine the 50% drop height using a go/no-go threshold level of 117 decibels. Friction sensitivity was measured with a BAM friction instrument determining the 50% load using the Neyer D-Optimal method. Electrostatic discharge/spark (ESD) sensitivity testing was performed on an ABL ESD instrument to determine the threshold initiation level (TIL).[41,42]

3. RESULTS AND DISCUSSION

3.1. Morphology and Particle Size Analysis. Class 5 RDX was used specifically for this work as the finest commercially available powder to compare to ultrafine spray-dried powders. Figure 1 shows SEM images of Class 5 RDX, and two spray-dried RDX samples at 1000× magnification to display the drastic differences in particle sizes when neat RDX is processed using the spray drying technique. In Figure 1a, the Class 5 RDX has a mixture of smaller particles (on the order of 1−5 μm) and larger particles ranging up to 30 μm diameter. Figure 1b shows RDX spray-dried using the ultrasonic nozzle. This nozzle produces a mixture of fine, micron-sized particles mixed with a range of larger particles ranging from 5 to 30 μm.

https://doi.org/10.1021/acsomega.2c07011
ACS Omega 2023, 8, 1514−1522

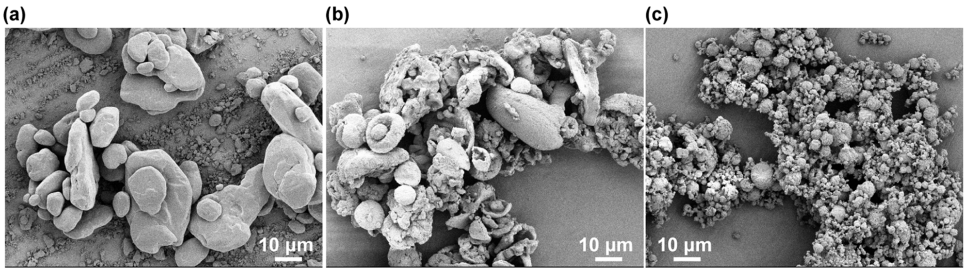

Figure 1. SEM images of (a) as-received Class 5 RDX, (b) spray-dried RDX using an ultrasonic nozzle, and (c) spray-dried RDX using a 0.7 mm atomizing nozzle.

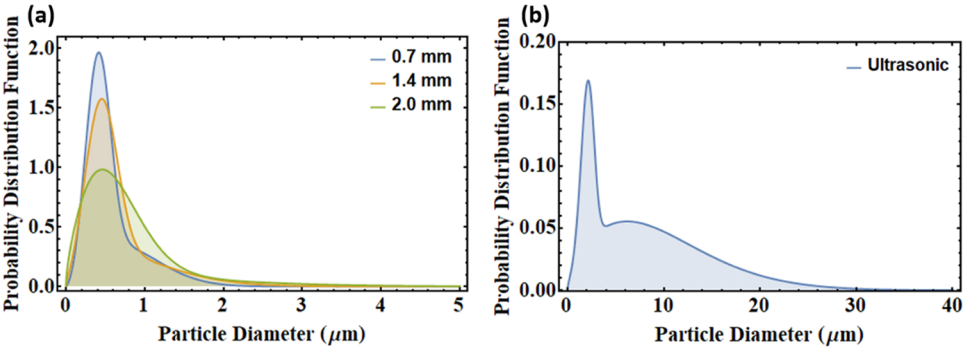

Figure 2. Particle size distributions for spray-dried RDX powders with various nozzle sizes and types. (a) PSD for spray-dried RDX using the three different sizes of atomizing nozzles, 0.7, 1.4, and 2.0 mm size openings. (b) PSD for spray-dried RDX using the ultrasonic nozzle.

Figure 1c shows RDX powder spray-dried with the smallest atomizing nozzle. This method produces mostly submicron particles with a few 1−2 μm particles. These SEM images clearly show the wide range of particle sizes and morphologies that spray drying provides.

To fully understand the level of control and accuracy of PSDs that spray drying offers, we spray-dried neat RDX with four nozzles. These nozzles consisted of three different size openings for the pneumatic nozzles, (0.7, 1.4, and 2.0 mm) as well as an ultrasonic nozzle. When spray drying with the different nozzles, all of the processing conditions including temperature and gas flow were kept as close as possible to each other to directly compare the effects of different nozzle sizes and types. The PSDs were calculated using high-resolution image analysis based on our previously reported methodology.[35] From the particle images, we measured and recorded particle areas using the built-in Keyence particle size analysis software, and constructed probability distribution functions to accurately represent the PSDs for each spray-dried powder. Figures S1 and S2 provide sample images that were taken using a Keyence VK-1000 and used for PSD analysis for each spray-dried RDX sample.

Figure 2a shows the probability distribution functions representing the PSDs for the spray-dried RDX using the three different sizes of pneumatic nozzles, while Figure 2b shows the PSD for the spray-dried RDX processed with the ultrasonic nozzle. The PSD statistics (average and standard deviation of particle diameter) for each sample are displayed in Table 1.

As seen in Figure 2a, the PSDs for each of the spray-dried samples are similar between the different sizes of pneumatic nozzles. However, the tail characteristics do slightly change between the nozzles. This demonstrates the ability to finely tune the powder PSD, where we can use the 0.7 mm nozzle to produce a nanopowder with a narrow PSD, or mix in various amounts of micron-sized particles by simply increasing the nozzle size to 1.4 or 2.0 mm. As shown in Figure 2a, the 0.7 mm nozzle provides the narrowest particle diameter distribution, with a maximum of 1.8 μm. When we increase the nozzle size to 1.4 mm, the main distribution is slightly wider, with an increase in the mode position. Also, we see a larger tail in this distribution with diameters up to 3.0 μm. Again, when we increase the nozzle to 2.0 mm, the main distribution becomes significantly wider than the smaller nozzles. We also observe that particles up to 5.0 μm are observed in the samples. Therefore, spray drying has proven to be a simple processing technique to produce ultrafine neat HE powders, which is highly sought after in the HE community to control energetic properties, as shown by the development of other HE processing techniques, such as fluid-energy milling (FEM), recrystallization, and rapid expansion of supercritical solutions (RESS).[43−46] Figure 2b shows the PSD of the ultrasonic spray-dried RDX. The pneumatic nozzles all have average particle diameters in the sub-μm range (0.57−0.81 μm average), while the ultrasonic nozzle has a particle diameter average of 8.20 μm. The particle size averages and standard deviations for each of the four spray-dried samples are presented in Table 2. This demonstrates the ability to spray-dry a neat RDX powder with about an order of magnitude larger PSD than the powders processed with the pneumatic nozzles. Additional statistics are

Table 2. Particle Size Distribution Statistics for the Spray-Dried RDX Powders

spray-dried RDX sample	average (μm)	standard deviation (μm)
0.7 mm nozzle	0.57	0.35
1.4 mm nozzle	0.64	0.45
2.0 mm nozzle	0.81	0.70
ultrasonic nozzle	8.20	6.30

https://doi.org/10.1021/acsomega.2c07011
ACS Omega 2023, 8, 1514−1522

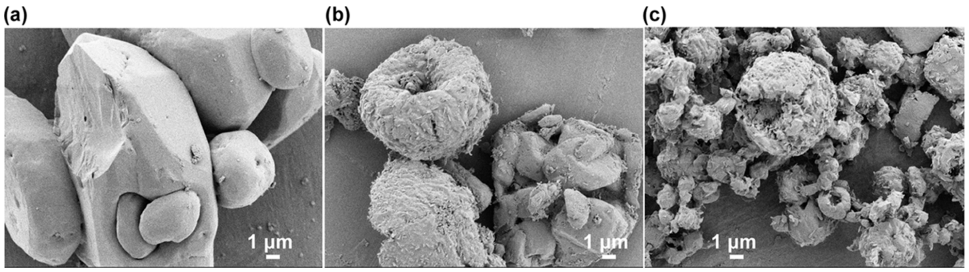

Figure 3. Representative SEM images at 5000× of (a) class 5 RDX, (b) ultrasonic spray-dried RDX, and (c) 0.7 mm atomizing spray-dried RDX powders for a closer look at crystal surface morphologies.

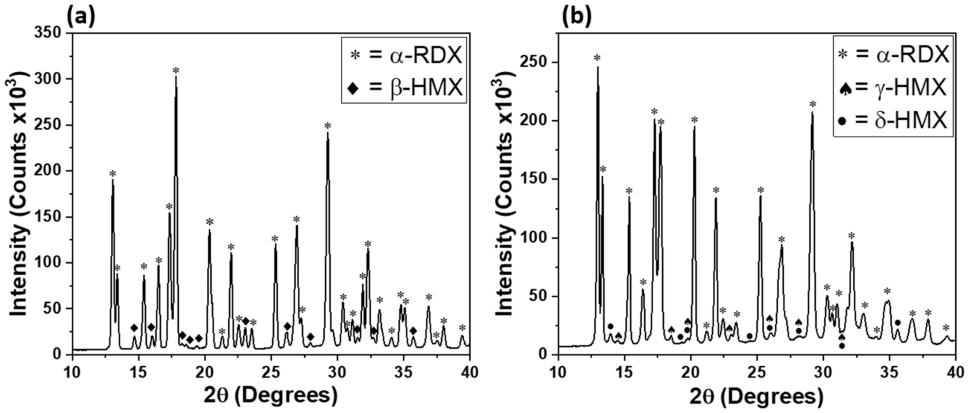

Figure 4. Powder XRD of (a) source class 5 RDX and (b) spray-dried RDX powders.

provided in Figure S3 to give supplementary visualization of the PSDs for the spray-dried RDX samples.

Because of the similarity in PSDs between the pneumatic nozzle sizes, we use the powder produced with the 0.7 mm nozzle as a representative ultrafine spray-dried RDX powder to compare to the ultrasonic spray-dried RDX and Class 5 RDX for all of the materials properties characterization in this work. Figure 3 shows another set of SEM images of the three powders from Figure 1. In these images, we increase the magnification to gain a better perspective on surface morphology differences between the source RDX and spray-dried RDX. Class 5 RDX is depicted in Figure 3a. The surface and edges of the source-material RDX crystals are relatively smooth. The ultrasonic spray-dried RDX, as shown in Figure 3b, has rounded edges, but the surface features show a mixture of rough and smooth regions between the crystals. The final spray-dried sample for comparison is shown in Figure 3c, which is the spray-dried RDX using the 0.7 mm pneumatic nozzle. The particles in this sample appear to have a greater degree of circularity without sharp edges. However, compared to the Class 5 and ultrasonic spray-dried RDX, the ultrafine spray-dried RDX consists of very rough surfaces with apparent defects in singular particles. The surface area of the different samples was also measured to further understand the changes in particle morphologies. As received, Class 5 RDX has the lowest surface area measured at 0.375 m^2/g. The RDX spray-dried with the ultrasonic nozzle has a surface area of 1.404 m^2/g. The RDX spray-dried with the 0.7 mm pneumatic nozzle has a surface area of 2.298 m^2/g. The surface area measurements help further understand how spray drying of HE powders can be useful for particle morphological control, where using different spray drying setups can modify particle size distributions, as well as surface area properties. Previous work has shown that other HE materials that are spray-dried, such as hexanitrostilbene (HNS) and PETN, have more spherical and smoother surface morphologies than the starting materials.[34,35] Therefore, it is clear that RDX behaves differently than other familiar materials when processed with spray drying, which could be an indication as to why RDX does not follow typical sensitivity trends as discussed later in this work.

3.2. Physical and Chemical Characterization. Powder XRD was performed to investigate if spray drying had any effect on the crystalline phase of the source RDX, as RDX is known to have a stable and second metastable polymorph at room temperature (α and β, respectively).[47−49] Figure 4 shows the powder XRD patterns comparing the source material (Class 5 RDX) to the ultrafine spray-dried RDX powder. The first important parameter from the XRD data shows that RDX retains the thermally stable, orthorhombic polymorph (α-RDX) after spray drying. It is important to show that processing RDX with this technique does not cause any undesirable polymorphism. However, as shown in Figure 4a, other peaks were observed in the XRD pattern for the class 5 RDX. This phase was hypothesized to be β-HMX, as it is well known that HMX impurities typically exist in RDX because the synthesis procedures for these two materials are very similar.[50] After indexing of the phase, it became clear that a small amount of HMX impurity was in the starting material. Previous work by Qiu et al. demonstrated that spray drying of HMX causes polymorphs to form due to a high degree of supersaturation during crystallization.[27,51,52] They determined that the thermally stable β-HMX forms two different polymorphs (γ and δ) after spray drying. In Figure 4b, we also show that the HMX impurity exists as the γ and δ after spray drying. While these forms are not desirable polymorphs for applications of HMX due to increased sensitivity and energy density,[14,53−55] the small amount of HMX in the RDX

https://doi.org/10.1021/acsomega.2c07011
ACS Omega 2023, 8, 1514−1522

(further quantified below) sample should not play a dominant role in small-scale sensitivity properties of the RDX.

The XRD patterns were also used to determine the average crystallite size and strain for the as-received Class 5 RDX and two samples of spray-dried RDX using the 0.7 mm nozzle and ultrasonic nozzle. The XRD whole pattern fitting results are shown in Table 3.

Table 3. XRD-Derived Crystallite Size and Strain for Select RDX Samples

sample	crystallite size (nm)	strain (%)
RDX Class 5	51 (1)	0
spray-dried (0.7 mm)	137 (2)	0.23 (1)
spray-dried (US)	654 (12)	0.21 (1)

The RDX Class 5 crystallite size falls within the range of published values and the zero strain is in line for solution-grown materials.[56] The spray-dried crystallite sizes are consistent with the SEM particle sizes, given that larger crystallite sizes will likely coalesce into larger particles. Differences in crystallite sizes between the two spray-dried samples are indicative of disparate crystallization mechanisms based on the two techniques and will require additional studies to understand. The strain values for the spray-dried material that underwent rapid crystallization are to be expected in terms of creating additional defects over traditional solution-grown crystals. It has been observed for HE materials such as RDX and HMX that lattice strain has a direct effect on the mechanical sensitivity of these materials.[18,57,58] Typically, an increase in microstrain of the lattice corresponds to a decrease in sensitivity to mechanical forces such as friction. This has been explained by various mechanisms, such as deformation twinning or dislocations improving the plasticity of the materials.[57,58]

To ensure that the HMX does not play a dominant role in small-scale sensitivity of the RDX before and after spray drying, ultrahigh-performance liquid chromatography (UHPLC) was used to quantify the concentration of HMX impurity in the RDX. The separation of RDX and HMX in Class 5 and spray-dried samples are shown in Figure 5. RDX exhibits more interaction with the UHPLC column and is therefore retained for a longer time period than the HMX. Therefore, in Figure 5, the first peak corresponds to the HMX, while the second peak corresponds to RDX. HMX concentrations in both Class 5 and spray-dried samples were measured based on the MRM parameters, as noted in Table 1. The Class 5 RDX contained 0.47 wt % HMX impurity, while the spray-dried RDX contained 0.55 wt % HMX impurity, with standard deviations of 0.012 and 0.024 wt %, respectively. While the difference in HMX concentration after spray drying is small, the change is statistically significant and requires further studies to fully understand if and how the total weight fraction of HMX changes after spray drying.

Figure 6 shows the DSC analysis of Class 5 and ultrafine spray-dried RDX samples. Typically, pure RDX is reported to have a melt temperature of ~205 °C, with an onset of decomposition shortly after melt at ~210 °C, which is shown by an endotherm directly followed by the exotherm in the DSC.[59,60] However, as shown in both the Class 5 and spray-dried RDX samples from this work, a double endotherm occurs, rather than the single endotherm that is typically observed for pure RDX. This is due to the existence of a β-HMX/RDX eutectic, which has a melt temperature of around 188−190 °C, as observed by the first endotherm in the DSC analysis.[12,61] The second endotherm that follows is the melt of the pure RDX, which is followed directly by the exothermic decomposition, making it difficult to quantify the exact temperature corresponding to the onset of decomposition.

3.3. Small-Scale Sensitivity. We investigated the impact of spray-dried PSDs and morphologies on the small-scale sensitivity of processed RDX powders. Table 4 summarizes the small-scale sensitivity data for the source RDX (Class 5) and the two spray-dried variants generated by the ultrasonic and 0.7 mm pneumatic nozzles. Three tests were used: drop weight impact, friction, and electrostatic discharge (ESD). All play an important role in determining the safety of HE powders.[42] In the drop weight impact test, a 2.5 kg weight is dropped onto a small powder sample of ~40 mg. Two microphones on either side of the apparatus measure the decibel (dB) output of the impact. If both microphones record 117 dB or greater, a reaction is recorded as a "go". Any measurement under 117 dB is considered a "no-go". Based on multiple drops, the height estimated to cause reaction 50% of the time is recorded as H_{50}. For this test, a greater height corresponds to more energy needed to cause reaction. In this measurement, we observe that the ultrasonic spray-dried RDX samples (25.5 cm) require a lower energy to cause a reaction via impact, or 15.6% height

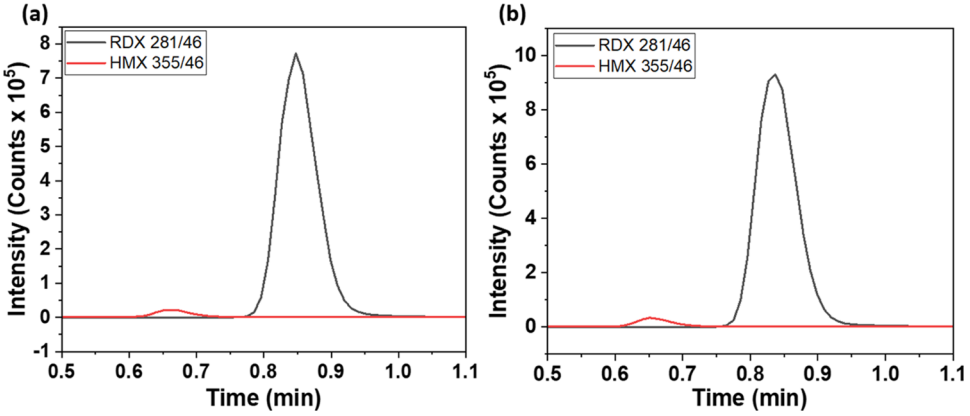

Figure 5. HPLC analysis of (a) class 5 and (b) spray-dried RDX powders. The different colored lines for HMX and RDX represent different mass channels that were recorded for each material.

https://doi.org/10.1021/acsomega.2c07011
ACS Omega 2023, 8, 1514−1522

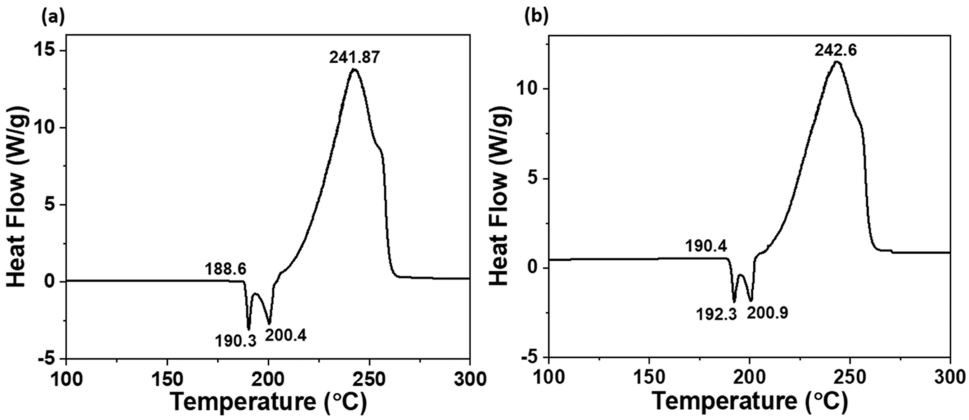

Figure 6. DSC analysis of (a) Class 5 and (b) spray-dried RDX powders.

Table 4. Small-Scale Sensitivity Results for the Three Different RDX Powders

		impact testing		friction testing		ESD testing
sample	average particle size (μm)	H_{50} (cm)	σ (cm)	50% load (N)	σ (cm)	TIL (J)
RDX − class 5	31.1[a]	30.2	1.0	>360	NA	0.125
RDX − spray-dried US	8.20	25.5	1.9	>360	NA	0.0625
RDX − spray-sried 0.7	0.57	22.8	2.7	296.9	76.2	0.125

[a]This value was taken from ref 39.

reduction compared to Class 5 RDX (30.2 cm). Between the two spray-dried samples, the ultrafine powder (22.8 cm, a 24.5% reduction compared to Class 5 RDX) also showed an increase in sensitivity by requiring even less energy to cause reaction. Compared to other commonly studied secondary energetic materials, such as the more sensitive PETN (average drop height, 11.8 cm) and the less sensitive triaminotrinitrobenzene (TATB), which has an average impact height of around 490 cm,[62,63] RDX has a drop height sensitivity closer to PETN. Therefore, the increase in impact sensitivity of RDX we observe after spray drying is not a drastic change and is still within the spectrum of standard response for secondary high explosives.

In a friction test, a small amount of powder is placed on a rigid plate. A pin is then placed on the covered plate and quickly dragged across the sample. Different weights can be hung on the end of the apparatus to increase the friction by applying more force to the pin. The operator then determines if the friction force causes reaction in the sample, via signatures of sound, smoke, and/or light. The force applied by the weight is recorded as the friction necessary to cause reaction. These results show the same order of sensitivity (ultrafine spray-dried RDX > ultrasonic spray-dried RDX ≥ Class 5 RDX) as the sensitivity determination from the impact results, showing that both the Class 5 RDX and the ultrasonic spray-dried RDX samples did not undergo any reactions under the maximum friction force (>360 N). The ultrafine spray-dried RDX was the only sample to undergo reaction in the friction test, with an average of 296.9 N.

The final sensitivity test is ESD testing. In this test, a sample is loaded into a small hole in a plastic sample holder. The sample is covered with a thin piece of tape and a spark is induced on the sample at various small levels. If the tape is broken after the spark is induced, then a reaction is recorded, whereas if the tape is still intact, then no reaction occurred from the spark in the material. With this experiment, we observed that all of the RDX samples had similar ESD thresholds of 0.125 J.

As mentioned previously, sensitivity control is important when working with HE materials. For instance, reducing particle size has been demonstrated as a common strategy for reducing the sensitivity of most high explosives.[17,64−66] However, recent studies have suggested that there are exceptions and inconsistencies in this strategy on the nanoscale.[36,37] Interestingly, both of these previous studies, as well as this work, focus on RDX, which may indicate that RDX behaves differently than other HE materials when reprocessing on the nanoscale. In our observations, we demonstrate that this difference in sensitivity properties of ultrafine RDX powder is likely due to surface morphology changes, as shown by SEM imaging, where the spray-dried RDX powders exhibit very rough surface features compared to the smoother Class 5 RDX source material.

4. CONCLUSIONS

We have demonstrated the use of spray drying to tune and control particle size distributions for processing of neat RDX on the micro- and nanoscale, primarily by changing the nozzle sizes and types. Using RDX as the material of interest in this work, we observed that spray drying alters the surface morphology such that rough surface features are produced relative to the starting material (class 5 RDX). This phenomenon appears to be distinct to RDX, as other HE materials have been spray-dried with smooth features, such as PETN and HNS. With detailed analysis via powder XRD and UHPLC, we determined that RDX remains in the thermally stable, orthorhombic polymorph (α-RDX) and that HMX impurities exist at a low concentration (around 0.5 wt %). Retaining the thermally stable polymorph after recrystallization processes is important to ensure sensitivity and performance characteristics do not drastically change, as polymorphism of HE materials can lead to increased sensitivity with decreased performance. Using XRD data analysis on crystalline strain, we

https://doi.org/10.1021/acsomega.2c07011
ACS Omega 2023, 8, 1514−1522

also observed that the spray drying process yields a small amount of strain, (~0.2%) which can also affect HE sensitivity. Microstrain has previously been shown to be inversely proportional to sensitivity, which is opposite of the increase in sensitivity observed in our study. This is likely due to other sensitivity factors being more dominant compared to the small amount of microstrain that occurs after spray drying, such as the nanocrystalline materials, surface roughness of the particles leading to a change in void structure, and the polymorphism of HMX contaminant to a more sensitive polymorph after spray drying. DSC showed a double endotherm, indicative of the RDX/HMX eutectic melt, and XRD showed that the process of spray drying changes the HMX impurity from β-HMX to γ- and δ-HMX polymorphs, as previously discovered. In contrast to the common strategy of reducing the sensitivity of HE materials by reducing particle size, we observed that the nanosized RDX powders increased in small-scale sensitivity relative to the Class 5 starting material, which we attribute to increased surface roughness and the nature of nanoparticle RDX.

■ ASSOCIATED CONTENT

Supporting Information

The Supporting Information is available free of charge at https://pubs.acs.org/doi/10.1021/acsomega.2c07011.

Microscope images of all samples that were used to calculate particle size distributions and additional statistical data for each sample particle size distribution (PDF)

■ AUTHOR INFORMATION

Corresponding Authors

Jeremy T. Tisdale − *High Explosives Science and Technology Q-5, Los Alamos National Laboratory, Los Alamos, New Mexico 87545, United States;* orcid.org/0000-0001-7281-9021; Email: jtisdale@lanl.gov

Amanda L. Duque − *High Explosives Science and Technology Q-5, Los Alamos National Laboratory, Los Alamos, New Mexico 87545, United States*; Email: aduque@lanl.gov

Authors

Brian L. Scott − *Materials Synthesis and Integrated Devices MPA-11, Los Alamos National Laboratory, Los Alamos, New Mexico 87545, United States*

Chris E. Freye − *High Explosives Science and Technology Q-5, Los Alamos National Laboratory, Los Alamos, New Mexico 87545, United States;* orcid.org/0000-0003-2634-1324

Larry G. Hill − *High Explosives Science and Technology Q-5, Los Alamos National Laboratory, Los Alamos, New Mexico 87545, United States*

Complete contact information is available at: https://pubs.acs.org/10.1021/acsomega.2c07011

Author Contributions

The manuscript was written through contributions of all authors. All authors have given approval to the final version of the manuscript.

Notes

The authors declare no competing financial interest.

■ ACKNOWLEDGMENTS

This work was supported by the US Department of Energy through the Los Alamos National Laboratory and the Dynamic Material Properties Program (Dana Dattlebaum, Program Manager). The authors thank Danielle Montanari, (SEM imaging) Lisa Klamborowski, (small-scale sensitivity testing), and Hongzhao Tian, (DSC measurements). Los Alamos National Laboratory is operated by Triad National Security, LLC, for the National Nuclear Security Administration of the U.S. Department of Energy (Contract No. 89233218NCA000001). Public release LA-UR-22-30162.

■ REFERENCES

(1) Masters, K. *Spray Drying: An Introduvtion to Principles, Operational Practice and Applications*; Leonard Hill: London, 1972.

(2) Patel, R. P.; Patel, M. P.; Suthar, A. M. Spray drying technology: an overview. *Indian J. Sci. Technol.* **2009**, *2*, 44−47.

(3) I Ré, M. Microencapsulation by Spray Drying. *Drying Technol.* **1998**, *16*, 1195−1236.

(4) Ameri, M.; Maa, Y.-F. Spray Drying of Biopharmaceuticals: Stability and Process Considerations. *Drying Technol.* **2006**, *24*, 763−768.

(5) Gharsallaoui, A.; Roudaut, G.; Chambin, O.; Voilley, A.; Saurel, R. Applications of spray-drying in microencapsulation of food ingredients: An overview. *Food Res. Int.* **2007**, *40*, 1107−1121.

(6) Reineccius, G. A. The Spray Drying of Food Flavors. *Drying Technol.* **2004**, *22*, 1289−1324.

(7) Vehring, R. Pharmaceutical Particle Engineering via Spray Drying. *Pharm. Res.* **2008**, *25*, 999−1022.

(8) Anandharamakrishnan, C.; Ishwarya, P. *Spray Drying Techniques for Food Ingredient Encapsulation*; John Wiley & Sons, Ltd.: Chicago, IL, 2015.

(9) Mang, J. T.; Skidmore, C. B.; Hjelm, R. P.; Howe, P. M. Application of small-angle neutron scattering to the study of porosity in energetic materials. *J. Mater. Res.* **2000**, *15*, 1199−1208.

(10) Greenaway, M. W.; Laity, P. R.; Pelikan, V. X-Ray Microtomography of Sugar and HMX Granular Beds Undergoing Compaction. *AIP Conf. Proc.* **2006**, *845*, 1279−1282.

(11) Wixom, R. R.; Tappan, A. S.; Brundage, A. L.; Knepper, R.; Ritchey, M. B.; Michael, J. R.; Rye, M. J. Characterization of pore morphology in molecular crystal explosives by focused ion-beam nanotomography. *J. Mater. Res.* **2010**, *25*, 1362−1370.

(12) Doherty, R. M.; Watt, D. S. Relationship Between RDX Properties and Sensitivity. *Propellants, Explos., Pyrotech.* **2008**, *33*, 4−13.

(13) Czerski, H.; Greenaway, M. W.; Proud, W. G.; Field, J. E. Links between the Morphology of RDX Crystals and their Shock Sensitivity. *AIP Conf. Proc.* **2006**, *845*, 1053−1056.

(14) Czerski, H.; Proud, W. G. Relationship between the morphology of granular cyclotrimethylene-trinitramine and its shock sensitivity. *J. Appl. Phys.* **2007**, *102*, No. 113515.

(15) van der Heijden, A. E. D. M.; Bouma, R. H. B.; van der Steen, A. C. Physicochemical Parameters of Nitramines Influencing Shock Sensitivity. *Propellants, Explos., Pyrotech.* **2004**, *29*, 304−313.

(16) Spyckerelle, C.; Eck, G.; Sjöberg, P.; Amnéus, A.-M. Reduced Sensitivity RDX Obtained From Bachmann RDX. *Propellants, Explos., Pyrotech.* **2008**, *33*, 14−19.

(17) Teipel, U. Production of Particles of Explosives. *Propellants, Explos., Pyrotech.* **1999**, *24*, 134−139.

(18) Teipel, U. *Energetic Materials Particle Processing and Characterization*. WILEY-VCH Verlag GmbH & Co.: Weinheim, Germany, 2005.

(19) Kumar, R.; Siril, P.; Soni, P. Preparation of Nano-RDX by Evaporation Assisted SolventAntisolvent Interaction. *Propellants, Explos., Pyrotech.* **2014**, *39*, 383−389.

(20) Kumar, R.; Siril, P. F.; Soni, P. Tuning the particle size and morphology of high energetic material nanocrystals. *Defence Technol.* **2015**, *11*, 382−389.
(21) Ji, W.; Li, X.; Wang, J. Preparation and Characterization of CL-20/EPDM by a Crystal Refinement and Spray Drying Method. *Cent. Eur. J. Energ. Mater.* **2015**, *12*, 831−840.
(22) Qiu, H.; Stepanov, V.; Di Stasio, A. R.; Surapaneni, A.; Lee, W. Y. Investigation of the crystallization of RDX during spray drying. *Powder Technol.* **2015**, *274*, 333−337.
(23) Qiu, H.; Stepanov, V.; Di Stasio, A. R.; Chou, T.; Lee, W. Y. RDX-based nanocomposite microparticles for significantly reduced shock sensitivity. *J. Hazard. Mater.* **2011**, *185*, 489−493.
(24) Patel, R. B.; Stepanov, V.; Swaszek, S.; Surapaneni, A.; Qiu, H. Investigation of HMX-Based Nanocomposites. *Propellants, Explos., Pyrotech.* **2015**, *40*, 210−214.
(25) Qiu, H.; Stepanov, V.; Patel, R. B.; Samuels, P.; Maier, K. H. Preparation and Characterization of Nanoenergetics Based Composition B. *Propellants, Explos., Pyrotech.* **2017**, *42*, 1309−1314.
(26) Ma, Z.; Gao, B.; Wu, P.; Shi, J.; Qiao, Z.; Yang, Z.; Yang, G.; Huang, B.; Nie, F. Facile, continuous and large-scale production of core−shell HMX@TATB composites with superior mechanical properties by a spray-drying process. *RSC Adv.* **2015**, *5*, 21042−21049.
(27) Qiu, H.; Stepanov, V.; Chou, T.; Surapaneni, A.; Di Stasio, A. R.; Lee, W. Y. Single-step production and formulation of HMX nanocrystals. *Powder Technol.* **2012**, *226*, 235−238.
(28) Liu, N.; Duan, B.; Lu, X.; Mo, H.; Xu, M.; Zhang, Q.; Wang, B. Preparation of CL-20/DNDAP cocrystals by a rapid and continuous spray drying method: an alternative to cocrystal formation. *CrystEngComm* **2018**, *20*, 2060−2067.
(29) An, C.; Li, H.; Ye, B.; Wang, J. Nano-CL-20/HMX Cocrystal Explosive for Significantly Reduced Mechanical Sensitivity. *J. Nanomater.* **2017**, *2017*, No. 3791320.
(30) Stepanov, V.; Patel, R. B.; Mudryy, R.; Qiu, H. Investigation of Nitramine-Based Amorphous Energetics. *Propellants, Explos., Pyrotech.* **2016**, *41*, 142−147.
(31) Hou, C.; Li, C.; Jia, X.; Zhang, Y.; Zhang, S. Facile Preparation and Properties Study of CL-20/TATB/VitonA Composite Microspheres by a Spray-Drying Process. *J. Nanomater.* **2020**, *2020*, No. 8324398.
(32) Song, C.-g.; Li, X.-d.; Yang, Y.; Liu, H.-m.; Tan, Y.-x.; Wang, J.-y. Formation and characterization of core-shell CL-20/TNT composite prepared by spray-drying technique. *Defence Technol.* **2021**, *17*, 1936−1943.
(33) Ye, B. Y.; An, C. W.; Wang, J. Y.; Geng, X. H. Formation and properties of HMX-based microspheres via spray drying. *RSC Adv.* **2017**, *7*, 35411−35416.
(34) Shi, J.; Zhu, P.; Zhao, S.; Xu, C.; Yan, F.; Shen, R.; Xia, H.; Jiang, H.; Xu, S.; Zhao, F. Continuous spheroidization strategy for explosives with micro/nano hierarchical structure by coupling microfluidics and spray drying. *Chem. Eng. J.* **2021**, *412*, No. 128613.
(35) Tisdale, J. T.; Hill, L. G.; Duque, A. L. Production of desensitized, ultrafine PETN powder. *Powder Technol.* **2022**, *396*, 152−157.
(36) Klaumünzer, M.; Pessina, F.; Spitzer, D. Indicating Inconsistency of Desensitizing High Explosives against Impact through Recrystallization at the Nanoscale. *J. Energ. Mater.* **2017**, *35*, 375−384.
(37) Stepanov, V.; Anglade, V.; Balas Hummers, W. A.; Bezmelnitsyn, A. V.; Krasnoperov, L. N. Production and Sensitivity Evaluation of Nanocrystalline RDX-based Explosive Compositions. *Propellants, Explos., Pyrotech.* **2011**, *36*, 240−246.
(38) Stepanov, V.; Willey, T. M.; Ilavsky, J.; Gelb, J.; Qiu, H. Structural Characterization of RDX-Based Explosive Nanocomposites. *Propellants, Explos., Pyrotech.* **2013**, *38*, 386−393.
(39) Brown, G. W.; Sandstrom, M. M.; Preston, D. N.; Pollard, C. J.; Warner, K. F.; Sorensen, D. N.; Remmers, D. L.; Phillips, J. J.; Shelley, T. J.; Reyes, J. A.; Hsu, P. C.; Reynolds, J. G. Statistical Analysis of an Inter-Laboratory Comparison of Small-Scale Safety and Thermal Testing of RDX. *Propellants, Explos., Pyrotech.* **2015**, *40*, 221−232.
(40) Hegel, C.; Jones, C. A.; Cabrera, F. A.; Yanez, M. J.; Bucala, V. Particle Size Characterization: Comparison of Laser Diffraction (LD) and Scanning Electron Microscopy (SEM). *Acta Microscopia* **2014**, *23*, 11−17.
(41) Preston, D. N.; Brown, G. W.; Skidmore, C. B.; Reardon, B. L.; Parkinson, D. A. *Small-scale Explosives Sensitivity Safety Testing: A Departure from Bruceton*, Shock Compress. of Condens. Matter, Chicago, IL, AIP Conference Proceedings: Chicago, IL, 2012.
(42) Brown, G. W. *Small Scale Sensitivity Testing of Explosives at Los Alamos National Laboratory*; JANNAF: Vancouver, Washington, United States, Vancouver, Washington, United States, 2018.
(43) Stepanov, V.; Elkina, I. B.; Matsunaga, T.; Chernyshev, A. V.; Chesnokov, E. N.; Zhang, X.; Lavrik, N. L.; Krasnoperov, L. N. Production of nanocrystalline RDX by rapid expansion of supercritical solutions. *Int. J. Energ. Mater. Chem. Propul.* **2007**, *6*, 75−87.
(44) Kennedy, J. E.; Lee, K.-Y.; Son, S. F.; Martin, E. S.; Asay, B. W.; Skidmore, C. B. Second-harmonic generation and the shock sensitivity of TATB. *AIP Conf. Proc.* **2000**, *505*, 711−714.
(45) Welle, E. J.; Molek, C. D.; Wixom, R. R.; Samuels, P. Microstructural effects on the ignition behavior of HMX. *J. Phys.: Conf. Series* **2014**, *500*, No. 052049.
(46) Nandi, A. K.; Kasar, S. M.; Thanigaivelan, U.; Ghosh, M.; Mandal, A. K.; Bhattacharyya, S. C. Synthesis and Characterization of Ultrafine TATB. *J. Energ. Mater.* **2007**, *25*, 213−231.
(47) Gao, C.; Yang, L.; Zeng, Y.; Wang, X.; Zhang, C.; Dai, R.; Wang, Z.; Zheng, X.; Zhang, Z. Growth and Characterization of β-RDX Single-Crystal Particles. *J. Phys. Chem. C* **2017**, *121*, 17586−17594.
(48) Goldberg, I. G.; Swift, J. A. New Insights into the Metastable β Form of RDX. *Cryst. Growth Des.* **2012**, *12*, 1040−1045.
(49) Brady, J. J.; Argirakis, B. L.; Gordon, A. D.; Lareau, R. T.; Smith, B. T. Polymorphic Phase Control of RDX-Based Explosives. *Appl. Spectrosc.* **2018**, *72*, 28−36.
(50) Borne, L.; Ritter, H. HMX as an Impurity in RDX Particles: Effect on the Shock Sensitivity of Formulations Based on RDX. *Propellants, Explos., Pyrotech.* **2006**, *31*, 482−489.
(51) Surber, E.; Lozano, A.; Lagutchev, A.; Kim, H.; Dlott, D. D. Surface Nonlinear Vibrational Spectroscopy of Energetic Materials: HMX. *J. Phys. Chem. C* **2007**, *111*, 2235−2241.
(52) McCrone, W. C. Crystallographic data: 36. Cyclotetramethylene tetranitramine (HMX). *Anal. Chem.* **1950**, *22*, 1225−1226.
(53) Kohno, Y.; Maekawa, K.; Tsuchioka, T.; Hashizume, T.; Imamura, A. A relationship between the impact sensitivity and the electronic structures for the unique N—N bond in the HMX polymorphs. *Combust. Flame* **1994**, *96*, 343−350.
(54) Zhu, W.; Xiao, J.; Ji, G.; Zhao, F.; Xiao, H. First-Principles Study of the Four Polymorphs of Crystalline Octahydro-1,3,5,7-tetranitro-1,3,5,7-tetrazocine. *J. Phys. Chem. B* **2007**, *111*, 12715−12722.
(55) Song, X.; Wang, Y.; Chongwei, A.; Guo, X.; Li, F. Dependence of particle morphology and size on the mechanical sensitivity and thermal stability of octahydro-1,3,5,7-tetranitro-1,3,5,7-tetrazocine. *J. Hazard. Mater.* **2008**, *159*, 222−229.
(56) Erofeev, L. N.; Tarasov, Y. P.; Kalmykov, Y. B.; Shu, Y.; Dubikhin, V. V.; Nazin, G. M. Crystal defects and stability of RDX. *Russ. Chem. Bull.* **2001**, *50*, 1000−1002.
(57) Armstrong, R. W.; Ammon, H. L.; Du, Z. Y.; Elban, W. L.; Zhang, X. J. Energetic Crystal-Lattice-Dependent Responses. *MRS Proc.* **1992**, *296*, 227.
(58) Herrmann, M.; Forter-Barth, U.; Kempa, P. B. Size/Strain Diffraction Peak Broadening of the Energetic Materials FOX-7, RDX and ADN. *Cent. Eur.J.Energ. Mater.* **2009**, *6*, 183−193.
(59) Singh, G.; Siril, P.; Soni, P. Studies on energetic compounds: Part 31. Thermolysis and kinetics of RDX and some of its plastic bonded explosives. *Thermochim. Acta* **2005**, *426*, 131−139.
(60) Gao, W.; Liu, X.; Su, Z.; Zhang, S.; Yang, Q.; Wei, Q.; Chen, S.-P.; Xie, G.; Yang, X.; Gao, S. High-energy-density materials with remarkable thermostability and insensitivity: syntheses, structures and

https://doi.org/10.1021/acsomega.2c07011
ACS Omega 2023, 8, 1514−1522

physicochemical properties of Pb(II) compounds with 3-(tetrazol-5-yl) triazole. *J. Mater. Chem. A* **2014**, *2*, No. 11958.
(61) McKenney, R. L.; Krawietz, T. R. Binary Phase Diagram Series: HMX/RDX. *J. Energ. Mater.* **2003**, *21*, 141−166.
(62) Rice, B. M.; Hare, J. J. A Quantum Mechanical Investigation of the Relation between Impact Sensitivity and the Charge Distribution in Energetic Molecules. *J. Phys. Chem. A* **2002**, *106*, 1770−1783.
(63) Keshavarz, M. H.; Jaafari, M. Investigation of the Various Structure Parameters for Predicting Impact Sensitivity of Energetic Molecules via Artificial Neural Network. *Propellants, Explos., Pyrotech.* **2006**, *31*, 216−225.
(64) Kim, S.-J.; Lee, B.-M.; Lee, B.-C.; Kim, H.-S.; Kim, H.; Lee, Y.-W. Recrystallization of cyclotetramethylenetetranitramine (HMX) using gas anti-solvent (GAS) process. *J. Supercrit. Fluids* **2011**, *59*, 108−116.
(65) Risse, B.; Schnell, F.; Spitzer, D. Synthesis and Desensitization of Nano-β-HMX. *Propellants, Explos., Pyrotech.* **2014**, *39*, 397−401.
(66) Guo, X.; Ouyang, G.; Liu, J.; Li, Q.; Wang, L.; Gu, Z.; Li, F. Massive Preparation of Reduced-Sensitivity Nano CL-20 and Its Characterization. *J. Energ. Mater.* **2015**, *33*, 24−33.

https://doi.org/10.1021/acsomega.2c07011
ACS Omega 2023, 8, 1514−1522